A view-based approach for the reconstruction of optical properties of turbid media

Atul Srivastava*, H. S. Patel and P. K. Gupta

Laser Biomedical Applications and Instrumentation Division,
Raja Ramanna Centre for Advanced Technology, Indore 452 013, India

A view-based approach for the computation of updates of optical parameters of a turbid medium is discussed. The approach differs from conventionally employed reconstruction techniques in terms of implementation of the computed updates. Simulation studies in frequency domain for tissue phantoms approximated by slab geometry have been presented. Results of the study show that the proposed inversion scheme, wherein the projection data corresponding to each view has been handled individually, works well in predicting the presence of an inhomogeneity. A comparison with the reconstruction results of conventionally employed inversion schemes involving simultaneous handling of projection data from all the view angles shows that the accuracy of the proposed scheme in predicting the presence of single inhomogeneity is higher and the reconstruction is also relatively free of artifacts. On the other hand, in the presence of multiple inhomogeneities, though the simultaneous handling of all the views gives better reconstruction, the updates obtained by the proposed scheme can be employed as close a priori information about the approximate positions of the inhomogeneities, thereby reducing the overall dimension of the Jacobian matrix to be inverted and hence making the convergence faster.

Keywords: Diffuse optical tomography, image reconstruction, optical properties, turbid medium.

OVER the past decade, diffuse optical tomography (DOT) has emerged as a viable method for non-invasive measurements of optical properties of highly scattering media and monitoring of living tissues[1–3]. Since DOT presents a typical ill-posed inverse problem with a limited number of measurements, use of an appropriate reconstruction algorithm is important. Hence, there has been considerable interest in the development of fast and accurate reconstruction algorithms. An iterative Newton–Raphson algorithm was employed by Pogue et al.[4] for the reconstruction of optical parameter distribution using a multigrid finite difference solution of the frequency domain diffusion equation. Jiang et al.[5] used a finite element-based reconstruction algorithm under diffusion approximation to simultaneously reconstruct the images of both absorption and scattering coefficients. Model et al.[6] introduced an iterative reconstruction algorithm for near-infrared imaging by

*For correspondence. (e-mail: atulsr@cat.ernet.in)

means of time-domain data. The algorithm was based on the finite element method forward model and on an optimization strategy that made use of the full information contained in the time-resolved measurements. Gao *et al.*[7] introduced an iterative algorithm, wherein a Tikhonov–Miller regularization method was employed to handle the ill-posed Jacobian matrix of the forward operator. Ye *et al.*[8] presented an inversion algorithm, wherein artifacts due to the poor regularization were reduced by incorporation of a Bayesian framework.

In recent years, various approaches have been proposed to improve the spatial resolution and quantitative accuracy of reconstruction using a priori knowledge of the optical properties of the medium under study. It has been shown by various researchers that the use of a priori information leads to reduction in the overall solution domain by making it less sensitive to the noise in the measured data. Pogue and Paulsen[9] used a priori information about the structural data obtained from magnetic resonance imaging for near-infrared optical image reconstruction of rat cranium with high resolution. Dehghani *et al.*[10] demonstrated that the quantitative accuracy of imaging with near-infrared optical tomography could be significantly improved when a priori information regarding the internal structure of imaging domain is utilized. Some recent studies[11–13] have made use of known absorbance spectrum of chromophores as a priori information to improve the image quality and the degree of accuracy of reconstruction. With this spectral approach, the concentration of oxy-haemoglobin, decoy-haemoglobin, water and the scattering parameters can be recovered directly[14–17]. Recently, Srinivasan *et al.*[18] extended the use of spectral priors from 2D to 3D imaging. Previous studies using 3D models[19–21] have demonstrated that the method is qualitatively superior and an accurate localization of the inclusions is possible.

In majority of the studies discussed above, reconstruction algorithms employ the computation and inversion of full Jacobian matrix after each iteration. The resulting simultaneous handling of the projection data from all sources and detectors leads to high memory requirements and computational efforts. To overcome this difficulty, algebraic reconstruction methods, wherein each row of the Jacobian matrix is handled individually, was earlier reported by Arridge[22]. Recently, Kumar and Vasu[23] developed an iterative method for the reconstruction of optical properties of a low-scattering object. They demonstrated two different ways of handling projection data; either one view at a time (consequently reducing the computational time) or using all the views simultaneously with a full dataset. They demonstrated the importance of the availability of a priori information in reconstructing multiple inhomogeneities.

In the present work, applicability of the view-based method where projection data from one source and all detectors are handled at a time and updates of the optical parameters are computed for each view separately, is dis-

cussed. The updates corresponding to each view are independently computed using the initial guess of the field values of the optical properties of the turbid medium. Once all the individual updates are obtained, they are handled in two different ways: in the first case the updates are summed up (additive scheme) and in the second they are multiplied with each other (multiplicative scheme). The reconstruction results of these two approaches have been discussed in terms of accuracy in predicting the location of the embedded inhomogeneity and also in terms of the artifacts associated with the inversion of the Jacobian matrix. Single as well as multiple inhomogeneities have been considered with varying contrast levels (ratio of the optical properties of the embedded inhomogeneity and that of the otherwise homogeneous medium). Reconstruction results of the proposed scheme have been compared with those obtained using simultaneous handling of projection data from all the views.

Photon migration in the turbid medium under study has been modelled by the diffusion approximation of radiative transport equation in the frequency domain[4,24]:

$$[\nabla^2 + \kappa^2]\phi(r, \omega) = -\frac{c}{D} S(r, \omega), \tag{1}$$

where κ is the complex wave number given by

$$\kappa^2 = \frac{-c\mu_a + j\omega}{D} = 3\mu_s'\left(-\mu_a + j\frac{\omega}{c}\right).$$

Equation (1) has been discretized in the space domain using finite difference-based discretization scheme. The Robin (type III) boundary condition is used, which best describes the light interaction from a scattering medium to the external air boundary[25]. Simulations have been performed on tissue phantoms approximated by slab geometry (21 mm × 51 mm), as shown schematically in Figure 1. The physical domain has been discretized in 21×51 uniformly spaced grid points and hence the spacing between two consecutive grid points is equal to one transport length $(1/\mu_s')$. The op-
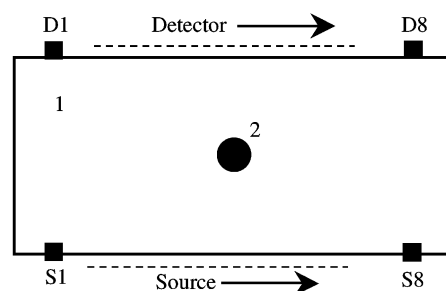
Figure 1. Schematic diagram of the turbid medium approximated by an infinite slab of finite thickness. The homogeneous medium is denoted by 1, whereas 2 denotes the absorbing inhomogeneity embedded in the medium.

tical properties of background medium have been kept close to that of living biological tissues. The absorption coefficient (μ_a), scattering coefficient (μ_s), and anisotropy parameter g are taken as 0.1 mm^{-1}, 10.0 mm^{-1} and 0.90 respectively. The reduced scattering coefficient ($\mu_s' = \mu_s(1 - g)$), thus becomes 1.0 mm^{-1}. Contrast levels of 2 : 1 and 5 : 1 between the embedded absorbing inhomogeneity and the otherwise homogeneous background medium have been considered. A combination of eight-sources and eight-detectors has been considered to scan the physical domain. Distribution of light emerging from the medium, which was illuminated with a source modulated at a frequency of 400 MHz, was computed numerically using the forward model. Measurements have been made in the transmission mode. For each source position, phase and ac amplitude were computed for all the detector locations, the source was traversed to its next location along the axial direction and the process was repeated. Hence a total of 128 measurements (64 amplitudes and phases each) were made. Since the reconstruction of only absorbing inhomogeneity has been considered in the present work, amplitude measurements have been employed as projection data. Random noise with 1% mean error was added to the simulated data to represent the experimental measurements.

The overall aim of the inverse imaging problem is to determine the values of optical parameters of the medium which provide a good fit between the measured (ϕ^{measured}) and simulated ($\phi^{\text{simulated}}$) data and require an iterative scheme. Minimization of the difference between the experimental and simulated data forms the basis of the inverse problem and can be defined by the following relationship:

$$[J]\{\Delta\mu_a, \ \Delta\mu_s\}^T = -\{\phi^{\text{measured}} - \phi^{\text{simulated}}\}. \tag{2}$$

Here $[J] = [\partial\phi/\partial\mu_a, \ \partial\phi/\partial\mu_s']$ is called the Jacobian matrix that describes the sensitivity of measurements to the perturbations in the optical properties of the medium. The elements of the Jacobain matrix can be computed using adjoint approach as[25]:

$$\left[\frac{\partial\phi^{\text{simulated}}}{\partial\mu_a}\right] = \frac{-c\Delta x\Delta z}{\mu_{a0}}G\phi^{\text{simulated}}, \tag{3}$$

and

$$\left[\frac{\partial\phi^{\text{simulated}}}{\partial\mu_s'}\right] = \frac{-c\Delta x\Delta z}{\mu_{s0}'}\nabla G \cdot \nabla\phi^{\text{simulated}}. \tag{4}$$

Here c is the speed of light in the medium and Δx and Δz are the spacings between two successive grid points in the x and z directions respectively. G is the Green's function due to a unit source at the detector positions on the

exit plane of the turbid medium and can be determined by solving the forward model with a unit source. $\phi^{\text{simulated}}$ is obtained from eq. (1) for known values of optical properties of the turbid medium. The elements of the Jacobian matrix $[J]$ can thus be fixed using eqs (3) and (4). The contour plot of the Jacobian matrix for a given source and detector position computed using adjoint approach is shown in Figure 2. In the present study, since the reconstruction of purely absorbing inhomogeneity has been considered, only eq. (3) has been used to fix the elements of the Jacobian matrix, as has earlier been done by Yalavarthy et al.[26].

For a given iteration, with the elements of the Jacobian matrix known, optical properties of the medium are determined by solving the inverse problem (eq. (2)). Since the Jacobian matrix involved in eq. (2) is close to singular (which makes it difficult to invert), eq. (2) is first multiplied by the transpose of the Jacobian to make it a square matrix, i.e.

$$[J]^T[J]\{\Delta\mu_a\}^T = [J]^T\{\phi^{\text{measured}} - \phi^{\text{simulated}}\}. \tag{5}$$

The square matrix given by eq. (5) has been solved using truncated singular value decomposition (tSVD) to determine the update values of the absorbing inhomogeneity for a given iteration. In both the cases (view-based approach and MOBIIR), the smallest singular value considered was kept fixed (1e-28). The guessed values of μ_a were then updated and further used to determine the fluence distribution ($\phi^{\text{simulated}}$) for the next iteration. The update vectors for the absorption coefficient $\{\Delta\mu_a\}$ for each view have been handled in two ways: updates from each view are either added (additive scheme) or multiplied with each other (multiplicative scheme) to form the final update. The perturbation equation was solved using tSVD approach. In each approach, a non-negativity constraint for the reconstructed optical parameters was enforced. In addition, we also used non-zero constraint in the proposed view-based multiplicative approach. The reconstruction results of these two approaches have been compared in terms of accuracy in predicting the presence of the inhomogeneity with the results of conventional reconstruction approaches currently in use, where updates from all the views are handled simultaneously. Contrast levels of 2 : 1 and 5 : 1 between the embedded inhomogeneities (single as
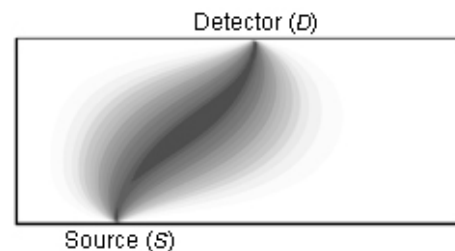
Figure 2. Sensitivity (Jacobian) contour plot for a source (S) and detector (D) position as computed using adjoint approach.
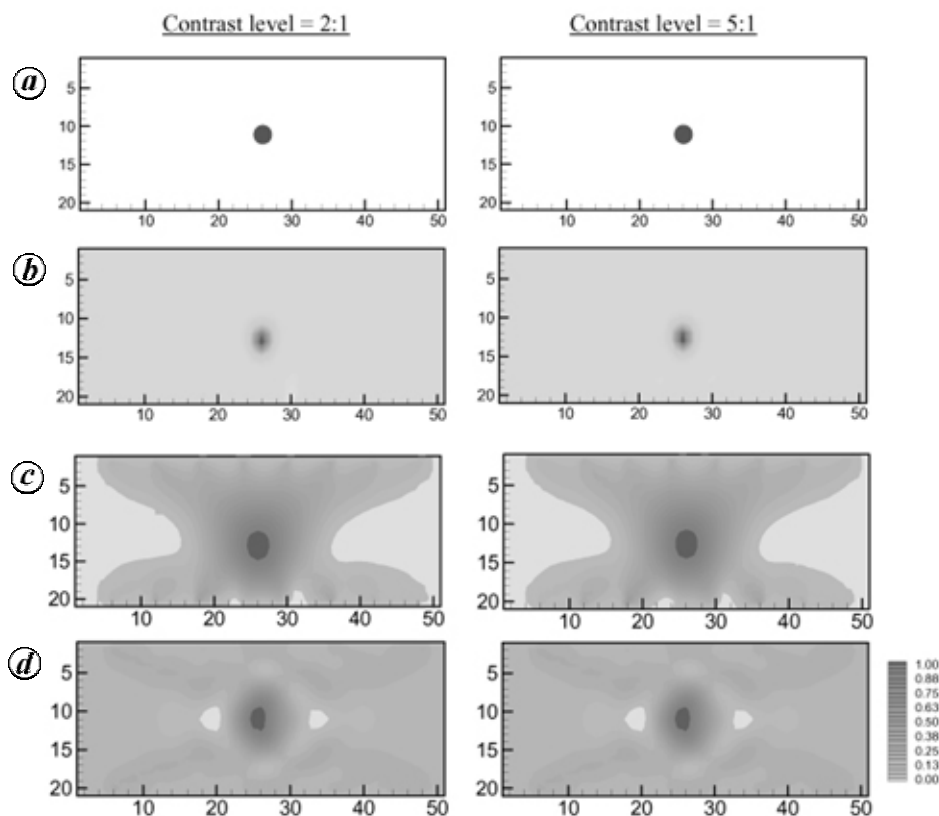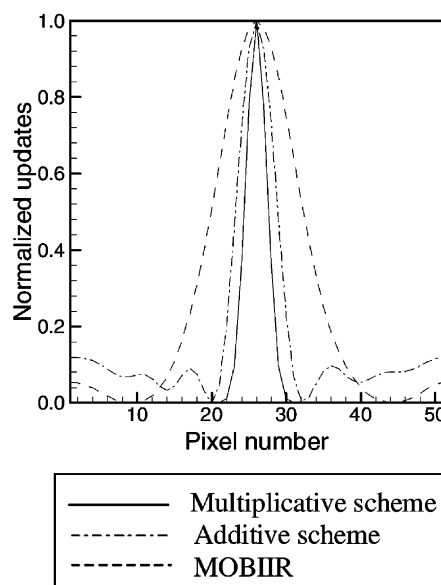
Figure 3. Reconstruction of absorbing inhomogeneity (schematically shown in *a*) embedded in a turbid medium for two contrast levels, 2 : 1 and 5 : 1. Results of two different inversion approaches (view-based and simultaneous handling of all the views) have been shown. *b*, View-based multiplicative scheme. *c*, View-based additive scheme. *d*, All views are simultaneously handled for inversion.

well as multiple) and the background medium have been considered.

Figure 3 demonstrates the reconstruction of single absorbing inhomogeneity (schematically shown in *a*) using the view-based approach, where update vectors from each view have been handled independently and are multiplied with each other (Figure 3 *b*) or added together (Figure 3 *c*) to form the final update. The reconstructed field obtained using the conventional method wherein updates from all the views were handled simultaneously is shown in Figure 3 *d*.

As can be seen from Figure 3, all the three approaches have been able to predict the presence of inhomogeneity (dark shade) quite accurately. However, the reconstructed fields obtained using the view-based additive scheme (Figure 3 *c*) and those obtained with the conventional method (Figure 3 *d*) show more pronounced artifacts compared to the proposed multiplicative scheme (Figure 3 *b*). It is interesting to note here that though the Jacobian matrix involved with the multiplicative scheme is mathematically more ill-conditioned (8×1071) than that encountered with the simultaneous handling of all the views (64×1071), there is considerable reduction in the degree of artifacts associated with the reconstructed field in the former case. This observation can be attributed to the way in which

Figure 4. Comparison of variation of normalized updates around the inhomogeneity along the width of the medium as obtained from the three reconstruction approaches. Central section passing through the region of inhomogeneity has been considered.

updates from each view are handled in the multiplicative scheme. Since the updates are being multiplied with each other, only those updates were preserved and further en-
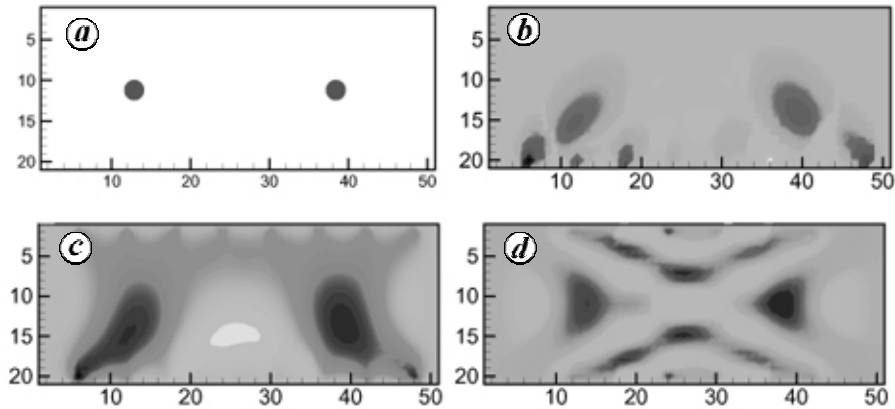
Figure 5. Reconstruction of multiple absorbing inhomogeneities (schematically shown in *a*) embedded in a turbid medium for a contrast level of 2 : 1. *b*, View-based multiplicative approach. *c*, View-based additive approach. *d*, All views are simultaneously handled (MOBIIR).

hanced that were localized in the region where the inhomogeneity was present, the rest being suppressed. Further, it should also be noted that there was considerable reduction in the computational time and memory requirement needed to invert relatively smaller size Jacobian matrix in the multiplicative scheme compared to that required in the conventional approaches where all the views are handled together. A closer comparison of the normalized updates around the location of the inhomogeneity as obtained from the three approaches is shown in Figure 4. The central section passing through the inhomogeneity has been considered. It can be seen that the updates obtained from the proposed view-based multiplicative scheme were strictly localized in the region of inhomogeneity and were zero otherwise, whereas updates from simultaneous handling of all the views were distributed to a wider region around the inhomogeneity and were non-zero in the rest of the medium which is otherwise homogeneous. Hence one can expect faster convergence of the proposed multiplicative scheme due to localization of updates just in the vicinity of the inhomogeneity.

Figure 5 shows the reconstruction of multiple absorbing inhomogeneities with the three inversion approaches. The location of these inhomogeneities has been schematically shown in Figure 5 *a*. Though the multiplicative (Figure 5 *b*) and additive (Figure 5 *c*) schemes predict the presence of inhomogeneities, a slight offset with respect to the original positions of the inhomogeneities can be seen in the reconstructed images. On the other hand, reconstruction using the conventional approach (MOBIIR) results in an accurate prediction of the positions of these inhomogeneities, as shown in Figure 5 *d*.

A quantitative comparison of these results, shown in Figure 6 where normalized updates from each inversion scheme were plotted, also reveals differences in the location of the inhomogeneities as predicted from the three approaches. This observation demonstrates the limitation
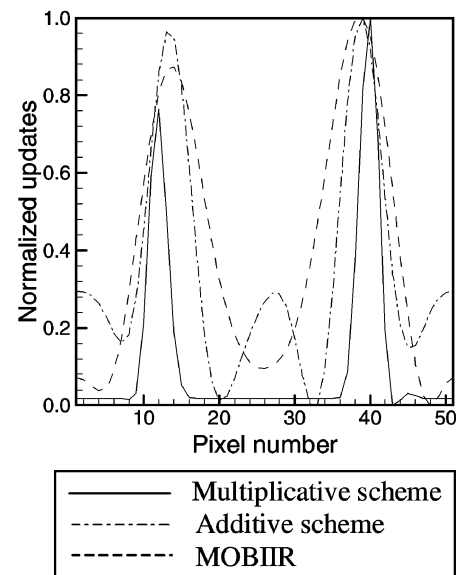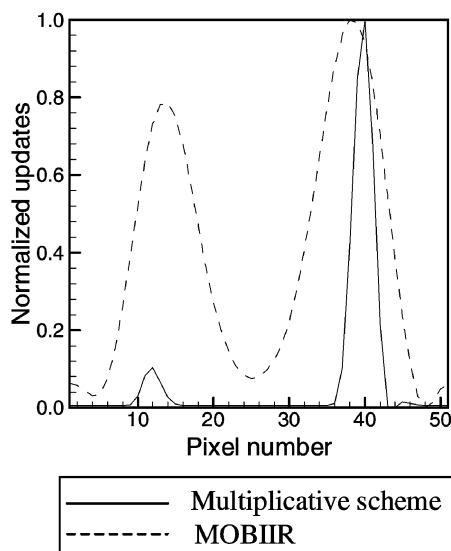

Figure 6. Comparison of variation of normalized updates around inhomogeneities along the width of the turbid medium as obtained from the three reconstruction approaches (contrast level = 2 : 1).

of the proposed view-based approach when applied to reconstruct multiple inhomogeneities present in a given turbid medium. However, the multiplicative scheme, being relatively free from artifacts and requiring less computational time, works well in predicting the approximate locations of the inhomogeneities, which in turn can serve as an acceptable a priori information. This a priori information about the positions of the inhomogeneties can be utilized for other conventional inversion approaches (e.g. MOBIIR where all the views are handled simultaneously) to reduce the dimension of the problem, leading to faster convergence.

Reconstruction of multiple inhomogeneities with varying contrast levels has also been performed using the three
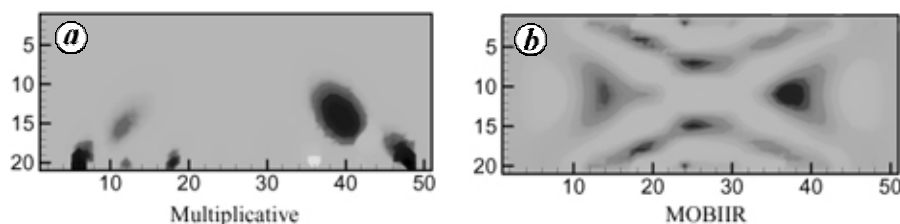
Figure 7. Reconstruction of multiple absorbing inhomogeneities with different contrast levels embedded in a turbid medium. Contrast levels are 2 : 1 (left) and 5 : 1 (right). *a*, View-based multiplicative approach. *b*, All views are simultaneously handled (MOBIIR).

Figure 8. Comparison of variation of normalized updates around the two inhomogeneities with different contrast levels for the three reconstruction schemes.

inversion approaches and the results are presented in Figure 7. Contrast levels of 2 : 1 and 5 : 1 were set for the left and the right inhomogeneities respectively. Reconstruction results of the view-based multiplicative scheme and the conventional approach (MOBIIR) have been compared. It is to be seen that though there is some mismatch between the reconstruction results of the two schemes in terms of predicting the accurate positions of the inhomogeneities with respect to the original objects (MOBIIR predicts the exact location, Figure 7 *b*), differences in the contrast levels of the two inhomogeneities have been brought out clearly in both the approaches, the left hand side inhomogeneity being of lighter shade in comparison to that present on the right.

This observation can also be made from Figure 8, where variation of normalized updates with respect to the width of the medium is plotted. Differences in the maximum values of the two peaks on either side of the centre line reveal the differences in contrast levels of the two inhomogeneities. Hence the reconstructed field shown in Figure 7 *a* demonstrates the potential of the proposed multiplicative scheme in terms of resolving different contrast levels of multiple inhomogeneties present in a given turbid medium.

The potential of a view-based approach, where projection data are handled one view at a time, has been explored in the present work and its applicability to reconstruct single and/or multiple absorbing inhomogeneities has been discussed. Updates corresponding to each view have been either added up (additive scheme) or multiplied with each other (multiplicative scheme). The method has the advantage of reduced memory requirements and computational time compared to other conventional schemes wherein projection data from all views are handled simultaneously. It has been shown in this study that the multiplicative view-based approach works well in predicting the presence of single absorbing inhomogeneity and the reconstructed field is almost free of artifacts associated with the inversion of the Jacobian matrix. On the other hand, the scheme is limited by the ill-posed Jacobian matrix, when applied to reconstruct multiple inhomogeneities and brings out only the approximate locations of the embedded objects. However, the reconstructed field in this case can be utilized as close a priori information about the approximate locations of the inhomogeneities and hence is useful to reduce the dimension of the Jacobian matrix to be inverted by other conventional approaches, where data from all the views are simultaneously handled, leading to faster convergence.

1. Yodh, A. and Chance, B., Spectroscopy and imaging with diffusing light. *Phys. Today*, 1995, **48**, 34–40.
2. Pogue, B. W., Testorf, M., McBride, T., Osterberg, U. and Paulsen, K., Instrumentation and design of a frequency-domain diffuse optical tomography imager for breast cancer detection. *Opt. Expr.*, 1997, **1**, 391–403.
3. Boas, D. A., Imaging the body with diffuse optical tomography. *IEEE Signal Process. Mag.*, 2001, **18**, 57–75.
4. Pogue, B. W., Patterson, M. S., Jiang, H. and Paulsen, K. D., Initial assessment of a simple system for frequency domain diffuse optical tomography. *Phys. Med. Biol.*, 1995, **40**, 1709–1729.
5. Jiang, H., Paulsen, K. D., Osterberg, U. L., Pogue, B. W. and Patterson, M. S., Simultaneous reconstruction of optical absorption and scattering maps in turbid media from near-infrared frequency-domain data. *Opt. Lett.*, 1995, **20**, 2128–2130.
6. Model, R., Orlt, M. and Walzel, M., Reconstruction algorithm for near-infrared imaging in turbid media by means of time-domain data. *J. Opt. Soc. Am. A*, 1997, **14**, 313–324.
7. Gao, F., Niu, H., Zhao, H. and Zhang, H., The forward and inverse models in time-resolved optical tomography imaging and their finite-element method solutions. *Image Vision Comput.*, 1998, **16**, 703–712.

8. Ye, J. C., Webb, K. J. and Bouman, C. A., Optical diffusion tomography by iterative coordinate-descent optimization in a Bayesian framework. *J. Opt. Soc. Am. A*, 1999, **16**, 2400–2412.

9. Pogue, B. W. and Paulsen, K. D., High-resolution near-infrared tomographic imaging simulations of the rat cranium by use of a priori magnetic resonance imaging structural information. *Opt. Lett.*, 1998, **23**, 1716–1718.

10. Dehghani, H., Pogue, B. W., Shudong, J., Brooksby, B. and Paulsen, K. D., Three-dimensional optical tomography: Resolution in small-object imaging. *Appl. Opt.*, 2003, **42**, 3117–3128.

11. Corlu, A., Durduran, T., Choe, R., Schweiger, M., Hillman, E. M., Arridge, S. R. and Yodh, A. G., Uniqueness and wavelength optimization in continuous-wave multispectral diffuse optical tomography. *Opt. Lett.*, 2003, **28**, 2339–2341.

12. Li, A., Zhang, Q., Culver, J. P., Miller, E. L. and Boas, D. A., Reconstructing chromosphere concentration images directly by continuous-wave diffuse optical tomography. *Opt. Lett.*, 2004, **29**, 256–258.

13. Srinivasan, S., Pogue, B. W., Jiang, S., Dehghani, H. and Paulsen, K. D., Spectrally constrained chromophore and scattering NIR tomography provides quantitative and robust reconstruction. *Appl. Opt.*, 2005, **44**, 1858–1869.

14. Hale, G. M. and Querry, M. R., Optical constants of water in the 200 nm to 200 μm wavelength region. *Appl. Opt.*, 1973, **12**, 555–563.

15. Boulnois, J. L., Photophysical processes in recent medical laser developments: A review. *Lasers Med. Sci.*, 1986, **1**, 47–66.

16. Staveren, H. J. V., Moes, C. J. M., Marle, J. V., Prahl, S. A. and Gemert, J. C. V., Light scattering in Intralipid – 10% in the wavelength range of 400–1100 nm. *Appl. Opt.*, 1991, **30**, 4507–4514.

17. Mourant, J. R., Fuselier, T., Boyer, J., Johnson, T. M. and Bigio, I. J., Predictions and measurements of scattering and absorption over broad wavelength ranges in tissue phantoms. *Appl. Opt.*, 1997, **36**, 949–957.

18. Srinivasan, S., Pogue, B. W., Dehghani, H., Leblond, F. and Intes, X., Data subset algorithm for computationally efficient reconstruction of 3-D spectral imaging in diffuse optical tomography. *Opt. Exp.*, 2006, **14**, 5394–5410.

19. Schweiger, M. and Arridge, S. R., Comparison of two- and three-dimensional reconstruction methods in optical tomography. *Appl. Opt.*, 1998, **37**, 7419–7428.

20. Hebden, J. C., Veenstra, H., Dehghani, H., Hillman, E. M., Schweiger, M., Arridge, S. R. and Delpy, D. T., Three-dimensional time-resolved optical tomography of a conical breast phantom. *Appl. Opt.*, 2001, **40**, 3278–3287.

21. Dehghani, H., Pogue, B. W., Shudong, J., Brooksby, B. and Paulsen, K. D., Three-dimensional optical tomography: Resolution in small-object imaging. *Appl. Opt.*, 2003, **42**, 3117–3128.

22. Arridge, S. R., Optical tomography in medical imaging. *Inverse Probl.*, 1999, **15**, R41–R91.

23. Kumar, Y. P. and Vasu, R. M., Reconstruction of optical properties of low-scattering tissue using derivative estimated through perturbation Monte-Carlo method. *J. Biomed. Opt.*, 2004, **9**, 1002–1012.

24. O'Leary, M. A., Boas, D. A., Chance, B. and Yodh, A. G., Experimental images of heterogeneous turbid media by frequency-domain diffusing-photon tomography. *Opt. Lett.*, 1995, **20**, 426–428.

25. O'Leary, Imaging with diffuse photon density waves, Ph D dissertation, 1996.

26. Yalavarthy, P. K., Dehghani, H., Pogue, B. W. and Paulsen, K. D., Critical computational aspects of near infrared circular tomographic imaging: Analysis of measurement number, mesh resolution and reconstruction basis. *Opt. Expr.*, 2006, **14**, 6113–6127.

Characterization of defensin (*Tfgd2*) from *Trigonella foenum-graecum*

Sudar Olli[1], Lalitha Guruprasad[2] and P. B. Kirti[1,*]

[1]Department of Plant Sciences, and
[2]School of Chemistry, University of Hyderabad, Hyderabad 500 046, India

Defensins are small cysteine-rich peptides with a size of 5–10 kDa, and some of them exhibit antifungal activity. We have cloned and sequenced a 219 bp coding region of the cDNA of a defensin from *Trigonella foenum-graecum*, designated as *Tfgd2* using primers designed on the basis of a defensin, *AlfAFP* from *Medicago sativa* and reverse transcription-PCR. We have cloned the 701 bp genomic region of the defensin that comprised two exons and one long intron. The deduced amino acid sequence of Tfgd2 was similar to AlfAFP, except for two amino acid substitutions. It has 50% homology with the antifungal defensin *Psd1* from *Pisum sativum*, whose NMR solution structure has been determined. The mature peptide has 45 amino acids, while the signal peptide comprised 27 amino acids. Southern analysis of the genomic DNA blot indicated that the defensins appear to be an oligo-gene family with at least two members in *Trigonella*. Purified peptide from *Escherichia coli* expression displayed inhibitory activity against broad-spectrum fungal pathogens, *Rhizoctonia solani* and *Fusarium moniliforme*.

Keywords: Antifungal activity, cysteine-rich peptide, defensin, *Trigonella foenum-graecum*.

AMONG the antimicrobial peptides (AMPs), plant defensins are particularly important for frontline host defense against fungal pathogens. They are thought to be members of small gene families and are rich in conserved cysteine residues. All members of this family adopt a comparable global fold centred on the $CS\alpha\beta$ motif, but relatively few amino acid residues are absolutely conserved between all members[1]. This motif is also found in insect defensins and scorpion neurotoxins[2–4]. Despite their structural similarity, plant defensins are highly varied in their primary amino acid sequences, with only eight structure-stabilizing Cys residues in common[5]. In many cases, small differences in amino acid sequence can predict the specificity of the role of defense[6]. Variation in the primary sequences may account for the different biological activities reported for plant defensins, including antifungal activity[7], antibacterial activity[8], protease activity[9], and α-amylase inhibitory activity[10].

We have cloned the genomic region of *Tfgd2* from *Trigonella foenum-graecum* using the genomic DNA with